Energy & Environmental Science

Cite this: *Energy Environ. Sci.*, 2012, **5**, 6923

www.rsc.org/ees

COMMUNICATION

A graphene–platinum nanoparticles–ionic liquid composite catalyst for methanol-tolerant oxygen reduction reaction†

Yueming Tan,[a] Chaofa Xu,[a] Guangxu Chen,[a] Nanfeng Zheng*[a] and Qingji Xie[b]

Received 17th February 2012, Accepted 26th March 2012
DOI: 10.1039/c2ee21411c

We report here that graphene-supported Pt nanoparticles impregnated with the ionic liquid [MTBD][bmsi] which is more oxygen-philic and less methanol-philic than the exterior aqueous solution can exhibit both enhanced electrocatalytic activity and excellent methanol tolerance for oxygen reduction reaction.

Direct methanol fuel cells (DMFCs) as a subcategory of proton-exchange fuel cells have received much attention due to a variety of advantages, such as low cost of the fuel, low operating temperature, easy transportation and storage of the fuel, high energy efficiency and low exhaustion, and the fast start-up of the fuel.[1–5] Pt is widely used as the cathode catalyst for oxygen reduction reaction (ORR) in DMFCs, but at least two important issues must be addressed before Pt-based catalysts can be commercialized for DMFC applications. One is the fact that the sluggish ORR kinetics require high loading of Pt in the cathode for acceptable power density. The other is that methanol can easily cross over from the anode to the cathode side through the polymer membranes of DMFCs, which can decrease the cathode potential and reduce fuel efficiency due to the methanol oxidation reaction on Pt. Therefore, the development of cathode catalysts with enhanced ORR activity and excellent methanol tolerance is highly desired for implementation in DMFCs.

Several strategies including alloying Pt with transition metals (*e.g.*, Ni, Fe, and Co),[6–15] constructing Pt-based heterogeneous nanocatalysts,[16–20] changing the morphology of Pt catalysts from zero-dimensional nanoparticles to one-dimensional nanostructures,[21–25] fabricating interior oxygen-philic nanoporous electrodes,[26] and searching for effective support materials,[27,28] have been developed to improve the ORR activity. To overcome the so-called methanol crossover, recent work was concentrated on searching for methanol-insensitive Pt-free and Pt-based catalytic materials. Several Pt-free catalysts such as transition-metal macrocycles, ruthenium-based chalcogenides, and palladium-based alloys show a methanol-tolerant capability while retaining catalytic activity for ORR.[29–32] However, Pt-free catalysts present less ORR activity and inferior long-term stability in comparison to Pt-based catalysts. Considerable progress has also been achieved in the synthesis of Pt-based catalysts for methanol-tolerant ORR.[33–40] For instance, Pt nanoparticles embedded in mesoporous carbon can be used for methanol-tolerant ORR.[33,34] Another successful example is that Pt nanoparticles grown on $CoSe_2$ nanobelts are insensitive to methanol crossover.[35] Despite the great efforts in synthesis of methanol-tolerant ORR catalysts, design and synthesis of catalysts with both enhanced ORR activity and excellent methanol tolerance are still challenging.

Graphene (GN) nanosheet, a two-dimensional carbon material with high surface area, high conductivity, and unique graphitized

[a]*State Key Laboratory for Physical Chemistry of Solid Surfaces and Department of Chemistry, College of Chemistry and Chemical Engineering, Xiamen University, Xiamen 361005, China. E-mail: nfzheng@xmu.edu.cn; Fax: +86 5922183047; Tel: +86 592 2186821*
[b]*Key Laboratory of Chemical Biology and Traditional Chinese Medicine Research (Ministry of Education of China), College of Chemistry and Chemical Engineering, Hunan Normal University, Changsha 410081, China*

† Electronic supplementary information (ESI) available: Experimental details and data. See DOI: 10.1039/c2ee21411c

Broader context

Over the past few decades, direct methanol fuel cells (DMFCs) have been considered a promising energy conversion technology with the advantages of high efficiency and environmental friendliness. Pt-based catalysts are the most efficient cathode catalysts for oxygen reduction reaction (ORR) in DMFCs, but at least two challenges including the sluggish ORR kinetics and the so-called methanol crossover still hinder their wide commercialization. This requires scientists to develop cathode catalysts with both enhanced ORR activity and excellent methanol tolerance. Here we report that impregnating an ORR catalyst with an ionic liquid (IL) which is more oxygen-philic and less methanol-philic than the exterior aqueous solution provides an easy entry to methanol-tolerant ORR. Graphene-supported Pt nanoparticles impregnated with the ionic liquid [MTBD][bmsi] exhibited enhanced electrocatalytic activity and methanol tolerance, indicating a promising cathode catalyst candidate for practical DMFC applications. The strategy reported here may be helpful for design and synthesis of catalysts with excellent selectivity for catalysis, electrocatalysis, and chemo/bio-sensing.

basal plane structure, should be a promising candidate for catalyst support.[41–44] For instance, GN nanosheets have been proven to be excellent cathodic catalyst supports, which can improve both the ORR activity and stability of Pt.[27] Recently, an ionic liquid (IL) [MTBD][beti] with high oxygen solubility has been used to fabricate an interior oxygen-philic nanoporous electrode to improve the ORR activity.[26] However, by introducing GN or IL to Pt catalysts, a remarkable improvement has been achieved solely in the ORR activity. To make ORR catalysts fit for practical DMFC applications, the development of new strategies to enhance both ORR activity and methanol tolerance is highly desirable.

Herein, we report that impregnating an ORR catalyst with an IL can provide an easy entry into methanol-tolerant ORR. Pt nanoparticles supported on GN nanosheets were synthesized and used as a model ORR catalyst. The GN–Pt hybrids impregnated with the [MTBD][bmsi] IL (Scheme 1a), which is hydrophobic, protic, with high oxygen solubility, and less methanol-philic than the exterior aqueous solution, can yield a robust GN–Pt–IL composite catalyst. As illustrated in Scheme 1b, methanol diffusion from the exterior aqueous solution to catalyst layer is forbidden, while oxygen and proton participating in the ORR is allowed. As a result, the as-prepared GN–Pt–IL composite catalyst exhibited both enhanced ORR activity and excellent methanol tolerance.

In this work, carboxylic GN nanosheets (Fig. 1a) were used as a template to prepare GN–Pt hybrids. The GN–Pt hybrids were prepared by reduction of platinum(II) acetylacetonate in the presence of GN under CO atmosphere (see ESI† for details). The prepared GN–Pt hybrids were determined by transmission electron microscopy (TEM). As shown in Fig. 1b–d, the surface of GN is composed of ultrahigh density Pt nanoparticles. The Pt nanoparticles have a narrow size distribution and an average size of 3.4 nm (Fig. S1†). The X-ray diffraction (XRD) pattern demonstrates the face centered cubic (fcc) structure of Pt (Fig. S2†), indicating the highly crystalline nature of the as-prepared Pt nanoparticles. In a synthesis of GN–Pt hybrids without using CO, Pt nanoparticles with serious aggregation were obtained on GN (Fig. S3†). This result indicates that CO can stabilize the Pt nanoparticles with small size, which is consistent with previous studies.[45–47] Thus, we have developed an efficient approach to prepare GN–Pt hybrids by the direct chemical reduction of Pt precursor in the presence of GN under CO atmosphere.

In our design concept, selecting a suitable impregnating material is the key step in the preparation of a highly active and methanol-tolerant composite ORR catalyst. The impregnating material must be hydrophobic, protic, with high oxygen solubility, and less methanol-philic than the exterior aqueous solution. The [MTBD][bmsi] IL can

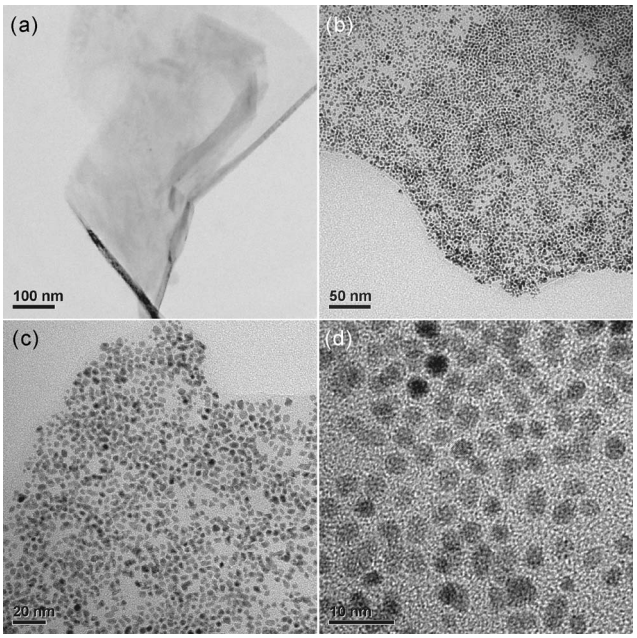

Fig. 1 TEM images of graphene nanosheets (a) and graphene–Pt hybrids (b–d) at different magnifications.

exhibit all of these characteristics due to its unique structure (Scheme 1a). (1) The perfluorinated side chains of the $[bmsi]^-$ anion make this IL hydrophobic. Experimentally, the [MTBD][bmsi] IL was mixed with water, and IL can be observed beneath water (photograph 1 of Fig. 2a). (2) The polarity difference between IL and methanol is much larger than that between methanol and water, so that methanol cannot diffuse easily from water to IL. Although methanol can dissolve in [MTBD][bmsi] IL (photograph 2 of Fig. 2a), methanol transfers rapidly into water from the IL after addition of water (photograph 3 of Fig. 2a). (3) The lone electron pairs on the nitrogen enable the IL to conduct protons and the perfluorinated side chains of the $[bmsi]^-$ anion give it an affinity for O_2,[26,48–50] so that ORR can take place on the surface of the Pt catalyst.

The GN–Pt–IL nanocomposite modified electrode can be obtained by simply placing a drop of IL on the GN–Pt hybrid modified electrode and rinsing off the unadsorbed IL with a stream of nitrogen. Similarly, GN–Pt–IL nanocomposites prepared on clean glass were collected for thermogravimetric analysis (TGA). TGA of GN–Pt–IL nanocomposites was conducted under N_2 atmosphere

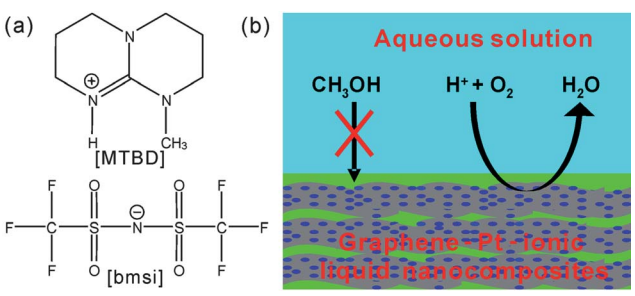

Scheme 1 (a) Structure of the [MTBD][bmsi] IL. (b) Illustration of methanol-tolerant ORR on graphene–Pt–ion liquid composite catalyst.

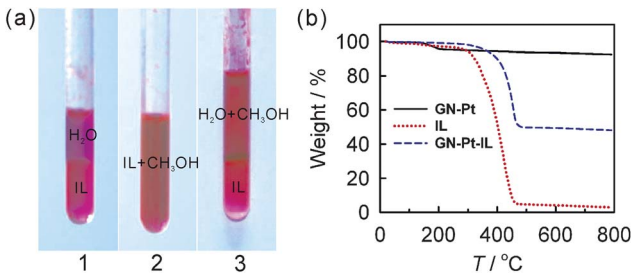

Fig. 2 (a) Mixture of H_2O + IL (1), IL + CH_3OH (2), and H_2O + CH_3OH + IL (3). All components with equal volume was used and each mixture was dyed with rhodamine B. (b) TGA profiles for GN–Pt hybrids, the [MTBD][bmsi] IL, and GN–Pt–IL composites.

and compared with that of GN–Pt hybrids and the [MTBD][bmsi] IL. As shown in Fig. 2b, the GN–Pt hybrids exhibit only 4% loss at 200 °C, resulting from the removal of the labile oxygen-containing functional groups. A significant weight loss is observed for the [MTBD][bmsi] IL above 300 °C, indicating that the thermal decomposition temperature of the [MTBD][bmsi] IL is considerably above the operating temperature of DMFCs. The GN–Pt–IL composites have a similar decomposition temperature as GN–Pt hybrids, indicating a large amount of IL impregnation in GN–Pt hybrids. In fact, owing to the hydrophobic interaction between the carbon material and ILs, ILs are widely used as binders for the construction of carbon paste electrodes.[51,52] It is expected that the unique two-dimensional structure and high surface area of GN nanosheets should be conducive to the entrapment of IL at high load.

The electrochemical behaviour of the GN–Pt–IL composite catalyst in 0.5 M H_2SO_4 was studied and compared with that of the GN–Pt catalyst. As shown in Fig. 3a, the hydrogen adsorption–desorption peaks on the GN–Pt–IL composite catalyst are similar to those on the GN–Pt catalyst, highlighting the protic nature of the [MTBD][bmsi] IL. A slight positive shift in the onset potential for Pt oxidation is observed for the GN–Pt–IL catalyst, indicating that surface oxidation of Pt was blocked to some extent in the presence of the [MTBD][bmsi] IL. The specific electrochemically active surface area (SEASA) was calculated by measuring the areas under the hydrogen adsorption–desorption peaks of the cyclic voltammograms, assuming that a monolayer of H ad-atoms requires 210 μC cm^{-2}. The SEASA of the GN–Pt–IL catalyst is calculated to be 60.5 m^2 g^{-1}, which is almost equal to that of the GN–Pt catalyst (61.3 m^2 g^{-1}) and a little smaller than that of commercial Pt–C (69.2 m^2 g^{-1}, 20 wt% Pt, E-TEK, Fig. S4a†).

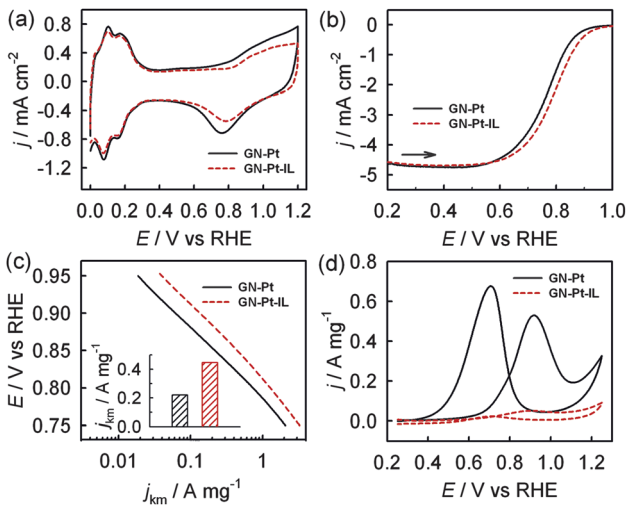

Fig. 3 (a) Cyclic voltammograms for GN–Pt and GN–Pt–IL catalysts in 0.5 M H_2SO_4 aqueous solution at 50 mV s^{-1}. (b) ORR polarization curves for GN–Pt and GN–Pt–IL catalysts recorded at room temperature in an O_2-saturated 0.5 M H_2SO_4 aqueous solution at a sweep rate of 10 mV s^{-1} and a rotation rate of 1600 rpm. (c) Mass activities (j_{km}) for these two catalysts, which are given as kinetic current densities (j_k) normalized to the Pt mass. Insets show the activities at 0.85 V. (d). Cyclic voltammograms of GN–Pt and GN–Pt–IL catalysts modified GCE in 0.5 M H_2SO_4 + 1 M CH_3OH solution at 50 mV s^{-1}, which are normalized to the Pt mass.

The ORR performances of GN–Pt and GN–Pt–IL catalysts in the absence of methanol were measured in O_2-saturated 0.5 M H_2SO_4 aqueous solution at room temperature using a rotating disk electrode (RDE). A characteristic set of polarization curves for the ORR on GN–Pt and GN–Pt–IL catalysts are displayed in Fig. 3b. Two distinguishable potential regions are clearly observed in the polarization curves: the well-defined diffusion limiting current region below 0.55 V and the mixed kinetic-diffusion control region between 0.6 and 0.95 V. The ORR polarization curves showed that the GN–Pt–IL catalyst has a more positive onset potential than the GN–Pt catalyst. In order to compare the activities of different catalysts, the kinetic currents in the kinetic-diffusion control regions, which are normalized to the Pt mass, are calculated from the ORR polarization curves by using mass-transport correction (Fig. 3c). The GN–Pt–IL catalyst shows a mass activity (j_{km}) of 0.45 A mg^{-1} at 0.85 V, which is 2.0 times that of the GN–Pt catalyst (0.22 A mg^{-1}). As well known, ORR kinetic currents are proportional to the oxygen activity at the catalyst surface.[53,54] So the enhanced ORR activity of the GN–Pt–IL catalyst should be ascribed to the high oxygen solubility of the [MTBD][bmsi] IL which impregnates the composite catalyst. Our result suggests that the ORR activity can be improved by introducing an interior oxygen-philic chemical environment to the nanoparticle catalyst system, though the availability of a similar strategy has been confirmed at an interior oxygen-philic nanoporous electrode.[26] The mass activity of the GN–Pt–IL catalyst is almost 3.2 times that of the commercial Pt–C catalyst (0.14 A mg^{-1}, Fig. S4b†). The corresponding specific activity of the GN–Pt–IL catalyst is 0.74 mA cm^{-2}, which is 3.7 times that of the commercial Pt–C catalyst (0.20 A mg^{-1}). The mass activity of the GN–Pt–IL catalyst at 0.9 V is also 3–4 times that of the GN–Pt nanocomposite and Pt–C catalysts reported previously (Table S1†).[27,55] As is well known, the ORR activity measured in the non-adsorbing electrolyte ($HClO_4$) is much higher than that in the adsorbing electrolyte (H_2SO_4).[53] As shown in Fig. S5† and Table S1†, the mass activity of the GN–Pt–IL catalyst in 0.1 M $HClO_4$ at 0.9 V is already 0.32 A mg^{-1}, which is much higher than that of various Pt–C catalysts.[56] Moreover, impregnating the Pt–Ni alloy catalyst with the [MTBD][bmsi] IL can yield a more active ORR catalyst. Experimentally, GN–Pt_3Ni hybrids were synthesized (Fig. S6†), and used to prepare the GN–Pt_3Ni–IL catalyst. The as-prepared GN–Pt_3Ni–IL catalyst shows a mass activity of 0.87 A mg^{-1} in 0.1 M $HClO_4$ at 0.9 V (Fig. S5†), which is 7.6 times that of the commercial Pt–C catalyst (0.11 A mg^{-1}). The GN–Pt_3Ni–IL catalyst is almost the most active ORR catalyst among Pt-based bimetallic catalysts reported previously (Table S1†).[7–9,14–16] It is worth noting here that the mass activity of the GN–Pt catalyst is also higher than that of the commercial Pt–C catalyst, indicating the advantage of using GN nanosheets as a cathode catalyst support. The stability test for the GN–Pt–IL catalyst was performed at room temperature in O_2-saturated 0.5 M H_2SO_4 solution by applying cyclic potential sweeps between 0.5 and 1.0 V at a sweep rate of 10 mV s^{-1} and a rotation rate of 1600 rpm for 500 cycles. As shown in Fig. S7†, there is only a slight loss in activity after the potential cycling, implying that the IL does not leak out easily and the composite catalyst is robust and stable.

Cyclic voltammetry was adopted to investigate the electrocatalytic performance of GN–Pt and GN–Pt–IL catalysts toward methanol oxidation. As shown in Fig. 3d, the GN–Pt catalyst exhibits high electrocatalytic activity for methanol oxidation while the GN–Pt–IL catalyst is inert for methanol oxidation. The methanol-tolerant ability

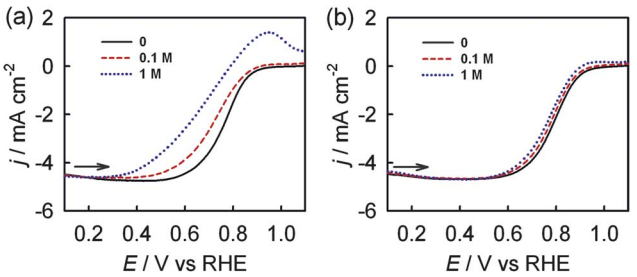

Fig. 4 ORR polarization curves for GN–Pt (a) and GN–Pt–IL (b) catalysts recorded at room temperature in O_2-saturated 0.5 M H_2SO_4 aqueous solution containing different concentrations of CH_3OH at a sweep rate of 10 mV s^{-1} and a rotation rate of 1600 rpm.

is attributed to the involvement of the [MTBD][bmsi] IL in the composite catalyst. Because the interior IL is less methanol-philic than the exterior aqueous solution, methanol diffusion from aqueous solution to the surface of Pt catalyst is forbidden.

The ORR performance of GN–Pt and GN–Pt–IL catalysts in the presence of methanol was also tested. Fig. 4 compares the effect of methanol on the ORR over the GN–Pt and GN–Pt–IL catalysts. The ORR on GN–Pt is seriously restrained in the presence of methanol even at a low concentration (0.1 M), due to the occurrence of methanol oxidation reaction on Pt. However, the ORR onset potential and current density for GN–Pt–IL catalyst remain almost unchanged in the presence of methanol at a concentration as high as 1 M. This finding suggests that the GN–Pt–IL catalyst is methanol-tolerant and can selectively perform the ORR in the presence of methanol, making the composite a promising cathode catalyst for practical DMFC applications.

In conclusion, monodisperse Pt nanoparticles grown on GN were synthesized with a simple approach and used as the electrocatalyst for ORR. Robust GN–Pt–IL nanocomposites were prepared by incubating GN–Pt hybrids with the [MTBD][bmsi] IL. Due to the hydrophobic, protic, less methanol-philic feature than the exterior aqueous solution, and high oxygen solubility characteristic of the [MTBD][bmsi] IL, the GN–Pt–IL composite catalyst exhibited both enhanced ORR activity and excellent methanol tolerance, indicating a promising cathode catalyst candidate for practical DMFC applications. The strategy reported here may be helpful for design and synthesis of catalysts with excellent selectivity for catalysis, electrocatalysis, and chemo/bio-sensing.

This work is supported by the MOST of China (2011CB932403, 2009CB930703), the NSF of China (21131005, 21021061, 20925103), the Fok Ying Tung Education Foundation (121011), and NSF of Fujian for a Distinguished Young Investigator Grant (2009J06005). Y. M. Tan also acknowledges the support of China Postdoctoral Science Foundation (20100480716).

Notes and references

1 X. Zhao, M. Yin, L. Ma, L. Liang, C. Liu, J. Liao, T. Lu and W. Xing, *Energy Environ. Sci.*, 2011, **4**, 2736.
2 E. Reddington, A. Sapienza, B. Gurau, R. Viswanathan, S. Sarangapani, E. S. Smotkin and T. E. Mallouk, *Science*, 1998, **280**, 1735.
3 M. S. Dresselhaus and I. L. Thomas, *Nature*, 2001, **414**, 332.
4 M. Winter and R. J. Brodd, *Chem. Rev.*, 2004, **104**, 4245.
5 G. S. Chai, I. S. Shin and J. S. Yu, *Adv. Mater.*, 2004, **16**, 2057.
6 V. R. Stamenkovic, B. Fowler, B. S. Mun, G. Wang, P. N. Ross, C. A. Lucas and N. M. Markovic, *Science*, 2007, **315**, 493.
7 J. Zhang, H. Yang, J. Fang and S. Zou, *Nano Lett.*, 2010, **10**, 638.
8 J. Wu, A. Gross and H. Yang, *Nano Lett.*, 2011, **11**, 798.
9 J. Wu, J. Zhang, Z. Peng, S. Yang, F. T. Wagner and H. Yang, *J. Am. Chem. Soc.*, 2010, **132**, 4984.
10 V. R. Stamenkovic, B. S. Mun, M. Arenz, K. J. J. Mayrhofer, C. A. Lucas, G. Wang, P. N. Ross and N. M. Markovic, *Nat. Mater.*, 2007, **6**, 241.
11 S. Mukerjee, S. Srinivasan and M. P. Soriaga, *J. Electrochem. Soc.*, 1995, **142**, 1409.
12 M. Watanabe, K. Tsurumi, T. Mizukami, T. Nakamura and P. Stonehart, *J. Electrochem. Soc.*, 1994, **141**, 2659.
13 S. Koh, J. Leisch, M. F. Toney and P. Strasser, *J. Phys. Chem. C*, 2007, **111**, 3744.
14 Y. Tan, J. Fan, G. Chen, N. Zheng and Q. Xie, *Chem. Commun.*, 2011, **47**, 11624.
15 R. Wang, C. Xu, X. Bi and Y. Ding, *Energy Environ. Sci.*, 2012, **5**, 5281.
16 B. Lim, M. Jiang, P. H. Camargo, E. C. Cho, J. Tao, X. Lu, Y. Zhu and Y. Xia, *Science*, 2009, **324**, 1302.
17 Z. Peng and H. Yang, *J. Am. Chem. Soc.*, 2009, **131**, 7542.
18 Y. Kim, J. W. Hong, Y. W. Lee, M. Kim, D. Kim, W. S. Yun and S. W. Han, *Angew. Chem., Int. Ed.*, 2010, **49**, 10197.
19 K. M. Yeo, S. Choi, R. M. Anisur, J. Kim and I. S. Lee, *Angew. Chem., Int. Ed.*, 2011, **50**, 745.
20 K. A. Kuttiyiel, K. Sasaki, Y. Choi, D. Su, P. Liu and R. R. Adzic, *Energy Environ. Sci.*, 2012, **5**, 5297.
21 C. Koenigsmann, W. P. Zhou, R. R. Adzic, E. Sutter and S. S. Wong, *Nano Lett.*, 2010, **10**, 2806.
22 S. Sun, F. Jaouen and J. P. Dodelet, *Adv. Mater.*, 2008, **20**, 3900.
23 Z. Chen, M. Waje, W. Li and Y. Yan, *Angew. Chem., Int. Ed.*, 2007, **46**, 4060.
24 H. Zhou, W.-p. Zhou, R. R. Adzic and S. S. Wong, *J. Phys. Chem. C*, 2009, **113**, 5460.
25 C. Koenigsmann and S. S. Wong, *Energy Environ. Sci.*, 2011, **4**, 1161.
26 J. Snyder, T. Fujita, M. W. Chen and J. Erlebacher, *Nat. Mater.*, 2010, **9**, 904.
27 R. Kou, Y. Shao, D. Wang, M. H. Engelhard, J. H. Kwak, J. Wang, V. V. Viswanathan, C. Wang, Y. Lin, Y. Wang, I. A. Aksay and J. Liu, *Electrochem. Commun.*, 2009, **11**, 954.
28 V. T. T. Ho, C. J. Pan, J. Rick, W. N. Su and B. J. Hwang, *J. Am. Chem. Soc.*, 2011, **133**, 11716.
29 H. Cheng, W. Yuan and K. Scott, *Electrochim. Acta*, 2006, **51**, 466.
30 P. H. C. Camargo, Z. M. Peng, X. M. Lu, H. Yang and Y. N. Xia, *J. Mater. Chem.*, 2009, **19**, 1024.
31 H. A. Gasteiger, S. S. Kocha, B. Sompalli and F. T. Wagner, *Appl. Catal., B*, 2005, **56**, 9.
32 S. Yin, M. Cai, C. Wang and P. K. Shen, *Energy Environ. Sci.*, 2011, **4**, 558.
33 Z. H. Wen, J. Liu and J. H. Li, *Adv. Mater.*, 2008, **20**, 743.
34 W. C. Choi, S. I. Woo, M. K. Jeon, J. M. Sohn, M. R. Kim and H. J. Jeon, *Adv. Mater.*, 2005, **17**, 446.
35 M. R. Gao, Q. Gao, J. Jiang, C. H. Cui, W. T. Yao and S. H. Yu, *Angew. Chem., Int. Ed.*, 2011, **50**, 4905.
36 X. Li, Q. Huang, Z. Zou, B. Xia and H. Yang, *Electrochim. Acta*, 2008, **53**, 6662.
37 H. Wang, J. Liang, L. Zhu, F. Peng, H. Yu and J. Yang, *Fuel Cells*, 2010, **10**, 99.
38 H. Yang, N. Alonso-Vante, J. M. Léger and C. Lamy, *J. Phys. Chem. B*, 2004, **108**, 1938.
39 S. Tominaka and T. Osaka, *Adv. Phys. Chem.*, 2011, **2011**, 821916.
40 Z. Wu, Y. Lv, Y. Xia, P. A. Webley and D. Zhao, *J. Am. Chem. Soc.*, 2012, **134**, 2236.
41 X. L. Li, X. R. Wang, L. Zhang, S. W. Lee and H. J. Dai, *Science*, 2008, **319**, 1229.
42 A. K. Geim and K. S. Novoselov, *Nat. Mater.*, 2007, **6**, 183.
43 S. Guo, S. Dong and E. Wang, *ACS Nano*, 2010, **4**, 547.
44 X. Huang, Z. Yin, S. Wu, X. Qi, Q. He, Q. Zhang, Q. Yan, F. Boey and H. Zhang, *Small*, 2011, **7**, 1876.
45 B. Wu, N. Zheng and G. Fu, *Chem. Commun.*, 2011, **47**, 1039.
46 G. Chen, Y. Tan, B. Wu, G. Fu and N. Zheng, *Chem. Commun.*, 2012, **48**, 2758–2760.

47 S. H. Chang, M. H. Yeh, C. J. Pan, K. J. Chen, H. Ishii, D. G. Liu, J. F. Lee, C. C. Liu, J. Rick, M. Y. Cheng and B. J. Hwang, *Chem. Commun.*, 2011, 3864.
48 H. Luo, G. Baker, J. Lee, R. Pagni and S. Dai, *J. Phys. Chem. B*, 2009, **113**, 4181.
49 M. Gomes, J. Deschamps and D. Menz, *J. Fluorine Chem.*, 2004, **125**, 1325.
50 J. Wang and F. Lu, *J. Am. Chem. Soc.*, 1998, **120**, 1048.
51 D. Wei and A. Ivaska, *Anal. Chim. Acta*, 2008, **607**, 126.
52 G. Shul, J. Sirieix-Plenet, L. Gaillon and M. Opallo, *Electrochem. Commun.*, 2006, **8**, 1111.
53 A. Damjanovic and V. Brusic, *Electrochim. Acta*, 1967, **12**, 615.
54 N. M. Markovic, H. A. Gasteiger, B. N. Grgur and P. N. Ross, *J. Electroanal. Chem.*, 1999, **467**, 157.
55 Y. Garsany, O. A. Baturina and K. E. Swider-Lyons, *Anal. Chem.*, 2010, **82**, 6321.
56 H. A. Gasteiger, S. S. Kocha, B. Sompalli and F. T. Wagner, *Appl. Catal., B*, 2005, **56**, 9.